

# Failure of the conformal-map method for relativistic quantum billiards

Barbara Dietz<sup>1,2,\*</sup>

<sup>1</sup>*Center for Theoretical Physics of Complex Systems,  
Institute for Basic Science (IBS), Daejeon 34126, Korea*

<sup>2</sup>*Basic Science Program, Korea University of Science and Technology (UST), Daejeon 34113, Korea*

(Dated: April 22, 2025)

We demonstrate that the conformal-map method introduced by Robnik in 1984 for nonrelativistic quantum billiards is not applicable for the quantization of relativistic neutrino billiards (NBs) consisting of a massless non-interacting spin-1/2 particle confined to a two-dimensional domain. To be precise, we demonstrate in this work, that this method does not provide solutions of the associated Weyl (Dirac) equation, nor does it fulfill the boundary conditions imposed on the spinor eigenfunctions to ensure confinement of the particle to the domain of the billiard. We review in detail the wave equation, boundary conditions and quantization of NBs and derivation of relevant equations, to make the proof comprehensible for the general reader. Our results are corroborated with numerical results for non-relativistic and relativistic quantum billiards whose shapes depend on a parameter, which allows the study of the properties of their eigenstates as the classical dynamics experiences a transition from regular to chaotic dynamics.

## I. INTRODUCTION

Billiards have served since the 1980th as a paradigm model for theoretical, numerical and experimental investigations of aspects of quantum chaos [1–3]. In the classical limit they refer to a bounded two-dimensional domain, in which a point particle moves freely and is reflected specularly at the boundary and have the particular property that their dynamics can be controlled by their shape. Nonrelativistic quantum billiards (QBs) are governed by the Schrödinger equation for a free particle which is confined to the billiard domain by imposing on the wave functions the Dirichlet boundary condition (BC) [4–7], and can be realized experimentally with flat microwave cavities [5, 8–13]. In 1987 Berry and Mondragon proposed relativistic neutrino billiards [14] (NBs). These are governed by the Weyl (Dirac) equation for a spin-1/2 particle which is confined to the billiard area by imposing the BC that there is no outward current.

For the study of spectral properties of QBs and NBs generally complete sequences of several 1000th of eigenvalues are needed. Their determination can be intricate and may require sophisticated methods, especially when the classical dynamics is close to integrable implying that the spacings between adjacent eigenvalues may become much smaller than their mean value. Such methods have been developed for nonrelativistic billiards based on the finite-element method [15], which in the mean time has been elaborated considerably, and for high-lying eigenstates one involving the boundary norm [16]. The boundary-integral method (BIM) has been introduced in Ref. [17] for QBs, in [14] for massless NBs and for massive ones in [18, 19]. It originates from the Green theorem, which provides an exact integral equation for the eigenfunctions in the interior of a QB or NB in terms of those

on the boundary, that is, the associated BCs are incorporated. In principle it is applicable to arbitrary shapes and has been applied even to dielectric billiards with dielectric BCs [20], for which one has to deal with singularities, to determine 100000th of eigenvalues [21, 22], however, modifications might be needed, e.g., when there are inner corners [23]. In the presence of nearly degenerate eigenvalues one might have to struggle in both cases with missing levels. For that case an expanded BIM has been developed in Refs. [24, 25]. Yet, for NBs, the occurrence of nearly degenerate eigenvalues is considerably less an issue than for nonrelativistic ones, and can generally be removed when they originate from discrete rotational symmetries by separating into the associated symmetry classes [17, 26].

In [27] a conformal-map method (CMM) has been introduced for the quantization of QBs whose shapes are generated from a conformal mapping of the circle, which provides the solutions of the associated Schrödinger equation with high accuracy. The method uses an expansion in terms of the eigenstates of the corresponding circle QB, which complies with the Dirichlet BC along the boundary of the QB by construction. This CMM has been applied, e.g., in [28–31] to analyze relativistic quantum scars. We will demonstrate in this work, that the CMM does not provide the eigenstates of NBs, although the eigenvalues might be close to the exact ones for sufficiently small deformations of the circular NB.

## II. REVIEW OF NEUTRINO BILLIARDS

We consider two-dimensional neutrino billiards (NBs), that were introduced in Ref. [14]. A NB consists of a massless relativistic spin-1/2 particle moving in a bounded two-dimensional region and is described by the Weyl equation [32] for Weyl fermions, which is generally

---

\* bdietzp@gmail.com

referred to as Dirac equation,

$$\hat{H}_D \psi = c \hat{\boldsymbol{\sigma}} \cdot \hat{\mathbf{p}} \psi = E \psi, \quad \psi = \begin{pmatrix} \psi_1 \\ \psi_2 \end{pmatrix}. \quad (1)$$

Here,  $\hat{\mathbf{p}} = -i\hbar \nabla$  is the momentum of the particle,  $\hat{H}_D$  denotes the Dirac Hamilton operator,  $\hat{\boldsymbol{\sigma}} = (\hat{\sigma}_x, \hat{\sigma}_y)$ , and  $\hat{\sigma}_{x,y,z}$  are the Pauli matrices. The energy of the particle is  $E = \hbar ck$ , where  $k$  is the free-space wave vector. The particle is confined to the billiard domain by imposing the BC that the outward flux vanishes. Accordingly, the normal component of the local current, that is, of the expectation value of the current operator  $\hat{\mathbf{u}} = \nabla_{\mathbf{p}} \hat{H}_D = c \hat{\boldsymbol{\sigma}}$  is required to vanish along the boundary [33],

$$\mathbf{n} \cdot [\psi^\dagger \nabla_{\mathbf{p}} \hat{H}_{NB} \psi] = c \mathbf{n} \cdot [\psi^\dagger \hat{\boldsymbol{\sigma}} \psi] = 0. \quad (2)$$

We consider NBs whose domain  $\Omega$  can be defined in a cartesian coordinate system in polar coordinates,  $\mathbf{r} = [x(r, \varphi), y(r, \varphi)]$ , or in the complex plane,

$$w(r, \varphi) = x(r, \varphi) + iy(r, \varphi), \quad \varphi \in [0, 2\pi), \quad r \in [0, r_0] \quad (3)$$

with the boundary  $\partial\Omega$  at  $r = r_0$  denoted as  $w(\varphi) \equiv w(r = r_0, \varphi)$ . Then, the BC, Eq. (2), reads [14]

$$\psi_2(\varphi) = i\mu B(\varphi) e^{i\alpha(\varphi)} \psi_1(\varphi). \quad (4)$$

Here,  $\alpha(\varphi)$  is the angle of the outward-pointing normal vector  $\mathbf{n} = [\cos \alpha(\varphi), \sin \alpha(\varphi)]$  at  $w(\varphi)$  with respect to the  $x$  axis, and  $\mu = \pm 1$  determines the rotational direction of the current at the boundary. We use  $\mu = 1$  in the following and  $B(\varphi) = 1$  in accordance with Ref. [14].

The normal vector  $\mathbf{n}$  can be expressed in terms of the derivative  $dw(\varphi)/d\varphi = w'(\varphi)$ ,  $e^{i\alpha(\varphi)} = -i \frac{w'(\varphi)}{|w'(\varphi)|}$ , yielding the BC

$$\psi_2(\varphi) = \frac{w'(\varphi)}{|w'(\varphi)|} \psi_1(\varphi). \quad (5)$$

Here, we used that for fixed  $r = r_0$  we have  $w'(z) = -\frac{i}{r_0 e^{i\varphi}} w'(\varphi)$ . Note, that  $\frac{d\alpha(\varphi)}{d\varphi} = \kappa(\varphi) |w'(\varphi)|$ , with  $\kappa(\varphi)$  denoting the curvature of the boundary at  $\varphi$ .

We restrict throughout the work to NBs whose shapes are generated by a conformal mapping of the circle defined in terms of polar coordinates  $0 \leq r \leq r_0$  and  $0 \leq \varphi \leq 2\pi$  by a polynomial in  $z$ ,

$$w(z) = x(r, \varphi) + iy(r, \varphi) = \sum_{l \geq 0} c_l z^l, \quad z = r e^{i\varphi}, \quad (6)$$

for  $r \in [0, r_0]$ ,  $\varphi \in [0, 2\pi)$ ,  $w'(z) \neq 0$ . Here, the  $c_l$  are real or complex coefficients. For  $r < r_0$  and  $r = r_0$ ,  $w(z)$  parameterizes the billiard domain  $\Omega$  and boundary  $\partial\Omega$ , respectively. The transformation Eq. (3) from  $(x, y)$  to  $w(z = r e^{i\varphi})$  yields for the gradient in the complex plane

$$\frac{\partial}{\partial x} + i \frac{\partial}{\partial y} = \frac{1}{[zw'(z)]^*} \left( r \frac{\partial}{\partial r} + i \frac{\partial}{\partial \varphi} \right), \quad (7)$$

where the star  $*$  denotes complex conjugation, leading to the Dirac equation, which consists of coupled equations for the spinor components  $\psi_1(r, \varphi)$  and  $\psi_2(r, \varphi)$ ,

$$ik\psi_1(r, \varphi) = \frac{1}{[zw'(z)]} \left( r \frac{\partial}{\partial r} - i \frac{\partial}{\partial \varphi} \right) \psi_2(r, \varphi), \quad (8)$$

$$ik\psi_2(r, \varphi) = \frac{1}{[zw'(z)]^*} \left( r \frac{\partial}{\partial r} + i \frac{\partial}{\partial \varphi} \right) \psi_1(r, \varphi). \quad (9)$$

Using

$$\left( r \frac{\partial}{\partial r} + i \frac{\partial}{\partial \varphi} \right) z = 0, \quad (10)$$

yields for the Laplace operator resulting from the conformal map Eq. (6)

$$\left( \frac{\partial}{\partial x} - i \frac{\partial}{\partial y} \right) \left( \frac{\partial}{\partial x} + i \frac{\partial}{\partial y} \right) = \frac{1}{|w'(z)|^2} \Delta_{(r, \varphi)}, \quad (11)$$

where  $\Delta_{(r, \varphi)}$  is the Laplace operator in polar coordinates. On the other hand, applying the differential operator given in Eq. (7) to Eq. (8) and its complex conjugate to Eq. (9) gives for each spinor component a separate Schrödinger equation,

$$\Delta_{(r, \varphi)} \psi(r, \varphi) = -k^2 |w'(z)|^2 \psi(r, \varphi), \quad (12)$$

with  $\psi(r, \varphi) = \psi_1(r, \varphi)$  or  $\psi(r, \varphi) = \psi_2(r, \varphi)$ . Yet, when solving these wave equations, one needs to take into account that the components are linked through Eq. (8) or, equivalently, through Eq. (9), and along the boundary in addition through the BC Eq. (5).

Solutions of the Dirac equation (8) and (9) can be written in the coordinate system Eq. (3) in terms of a plane-wave expansion of the form [34],

$$\Phi_1(r, \varphi) = \sum_l a_l(k) i^l J_l(k|w(z)|) e^{il\theta(z)}, \quad (13)$$

where  $J_l(x)$  denotes the Bessel function of the first kind, the coefficients  $a_l(k)$  are complex or real and independent of  $(r, \varphi)$  and  $e^{i\theta(z)} = \frac{w(z)}{|w(z)|}$ . Namely, inserting this ansatz into Eqs. (8) and (9) yields with equations (S1), (S2) and (S3) in Sec. A for the second component

$$\Phi_2(r, \varphi) = \sum_l a_l(k) i^{l+1} J_{l+1}(k|w(z)|) e^{i(l+1)\theta(z)}, \quad (14)$$

and

$$\Delta_{(r, \varphi)} \Phi_{n+1}(r, \varphi) \equiv -k^2 |w'(z)|^2 \sum_l a_l(k) i^l J_{l+n}(k|w(z)|) e^{i(l+n)\theta(z)}, \quad n = 0, 1 \quad (15)$$

implying that both spinor components solve the Schrödinger equation for a free particle Eq. (12). To be an eigenstate of the NB with shape  $w(z)$ ,  $\Phi_{1,2}(r, \varphi)$

should fulfill at discrete values of  $k$  the BC Eq. (5). Finding such solutions can be a cumbersome task. A very efficient method, which is based on the BIM, is introduced in [14].

In [27] a quantization method has been proposed for the eigenstates of nonrelativistic QBs, whose shapes are given by a  $w(z)$  with the properties Eq. (6). These are governed by the nonrelativistic Schrödinger equation Eq. (12) subject to the Dirichlet BC. The ansatz for the eigenfunctions is given in terms of a linear combination of the orthogonal eigenfunctions of the circular QB. For a circular billiard with radius  $r_0$  the domain is described by Eq. (6) with  $w(z) = z$ ,  $|w(z)| = r$ ,  $e^{i\theta(z)} = e^{i\varphi}$ , and the boundary is given as  $w(\varphi) = r_0 e^{i\varphi}$  yielding for the normal-vector components  $e^{i\alpha(\varphi)} = e^{i\varphi}$ . The eigenvalues  $k_n$  are given as the zeros of the Bessel functions and the eigenfunctions  $\psi_n(r, \varphi)$  are given in terms of the Bessel functions,

$$J_n(\epsilon_{n,\nu} r_0) = 0, \quad \psi_{n,\nu}^{\epsilon,o}(r, \varphi) = J_{n,\nu}(\epsilon_{n,\nu} r) f_n^{\epsilon,o}(\varphi), \quad (16)$$

with  $\nu = 1, 2, \dots, n = 1, 2, \dots$ ,  $f_n^e(\varphi) = \cos(n\varphi)$  and  $f_n^o(\varphi) = \sin(n\varphi)$  for solutions that are symmetric and antisymmetric with respect to the  $x$  axis, respectively. The index  $\nu$  denotes the  $\nu$ th zero of  $J_n(\epsilon_{n,\nu} r_0)$  for a given index  $n$ . The ansatz used in [27, 35] for the solutions of the Schrödinger equation Eq. (12) with Dirichlet BCs along the boundary  $w(\varphi)$  reads

$$\psi(r, \varphi) = \sum_{n=-\infty}^{\infty} \sum_{\nu=1}^{\infty} \frac{c_{n,\nu}(k) N_{n,\nu}}{\epsilon_{n,\nu}} J_{|n|,\nu}(\epsilon_{n,\nu} r) e^{in\varphi}, \quad (17)$$

with  $N_{n\nu}^{-1} = \sqrt{\pi} |J'_{n,\nu}|$ ,  $c_{n,\nu}$  denoting the expansion coefficients and  $\epsilon_{n,\nu} = \epsilon_{-n,\nu}$ . These wave functions fulfill the Dirichlet BCs by construction. The eigenvalues and associated eigenstates are obtained by solving the eigenvalue problem

$$\hat{M} \mathbf{c} = \frac{1}{k^2} \mathbf{c}, \quad (18)$$

with matrix elements  $\mathcal{N}_{n\nu m\mu} \hat{M}_{n\nu m\mu}$  given by

$$\int_0^{r_0} r dr \int_0^{2\pi} d\varphi |w'(z)|^2 e^{i(n-m)\varphi} J_{|n|,\nu}(\epsilon_{n,\nu} r) J_{|m|,\mu}(\epsilon_{m,\mu} r), \quad (19)$$

where  $\mathcal{N}_{n\nu m\mu}^{-1} = \frac{N_{n\nu} N_{m\mu}}{\epsilon_{n,\nu} \epsilon_{m,\mu}}$ . In Sec. IV we demonstrate the efficiency of this method for the Africa QB [35]. In analogy to that quantization procedure, in Ref. [28] a similar method in terms of the eigenfunctions of a circular NB was proposed. However, this ansatz does not solve the Dirac equation, i.e., Eqs. (8) and (9) and does not provide the eigenstates of the corresponding NB, as proven in the following.

### III. THE FLAWS OF THE CMM FOR NEUTRINO BILLIARDS

The eigenvalues and eigenfunctions of the circular NB are obtained by imposing the BC Eq. (5) on

the ansatz Eq. (13) with the second component given in Eq. (14), leading to the quantization condition [14]

$$J_{m+1}(\kappa_{m,\mu}) = J_m(\kappa_{m,\mu}), \quad (20)$$

where  $\mu$  counts the number of eigenstates below  $k_{m,\mu}$  for a given total angular momentum  $m + \frac{1}{2}$ , that is, the  $\kappa_{m,\mu}$  are sorted as  $\kappa_{m,1} \leq \kappa_{m,2} \leq \dots$ . The associated eigenfunctions read

$$\Phi_{1m,\mu}(r, \varphi) = \mathcal{N}_{m,\mu} i^m J_m(\kappa_{m,\mu} r) e^{im\varphi}, \quad (21)$$

$$\Phi_{2m,\mu}(r, \varphi) = \mathcal{N}_{m,\mu} i^{m+1} J_{m+1}(\kappa_{m,\mu} r) e^{i(m+1)\varphi}.$$

The spinor eigenfunctions

$$\Phi_{m,\mu}(r, \varphi) = \begin{pmatrix} \Phi_{1m,\mu}(r, \varphi) \\ \Phi_{2m,\mu}(r, \varphi) \end{pmatrix} \quad (22)$$

are orthogonal to each other [14] [cf. Sec. A],

$$\int_0^{r_0} r dr \int_0^{2\pi} d\varphi \Phi_{m,\mu}(r, \varphi) \cdot \Phi_{n,\nu}(r, \varphi) = \delta_{n,m} \delta_{\nu,\mu}. \quad (23)$$

In analogy to Ref. [27] for the CMM the ansatz for the first spinor component consists of a superposition of the eigenfunctions of the circular NB,

$$\psi_1(r, \varphi) = \sum_{n=-\infty}^{\infty} \sum_{\nu=1}^{\infty} a_{n,\nu}(k) i^n J_n(r \kappa_{n,\nu}) e^{in\varphi} = \sum_j a_j(k) \Phi_{1j}(r, \varphi), \quad (24)$$

where the index  $j$  counts the number of eigenvalues below  $\kappa_{l(j),\lambda(j)}$ , that is, these are sorted by size,  $\kappa_{l(1),\lambda(1)} \leq \kappa_{l(2),\lambda(2)} \leq \dots$ . Note, that for circular NBs we have  $\kappa_{n,\nu} \neq \kappa_{-n,\nu}$  [14].

The ansatz for the second component,  $\psi_2(r, \varphi)$  is obtained by inserting  $\psi_1(r, \varphi)$  into the Dirac equation (9), from which the associated Schrödinger equations for the two spinor components, that are solved within the CMM, originate, yielding

$$[w'(z)]^* \psi_2(r, \varphi) = \sum_{n,\nu} b_{n,\nu}(k) i^{n+1} J_{n+1}(r \kappa_{n,\nu}) e^{i(n+1)\varphi} = \sum_j b_j(k) \Phi_{2j}(r, \varphi), \quad (25)$$

$$b_{n,\nu}(k) = \frac{\kappa_{n,\nu}}{k} a_{n,\nu}(k).$$

Hence, for  $k \neq \kappa_{n,\nu}$  and  $[w'(z)]^* \neq 1$ , that is, for shapes different from a circle we have  $\frac{1}{[w'(z)]^*} b_{n,\nu} \neq a_{n,\nu}$ , in contrast to the assumptions of [28]. Inserting this result into Eq. (8) yields for  $\psi_1(r, \varphi)$  the Schrödinger equation

$$\sum_{n,\nu} a_{n,\nu}(k) \kappa_{n,\nu}^2 i^n J_n(\kappa_{n,\nu} r) e^{in\varphi} = k^2 |w'(z)|^2 \sum_{n,\nu} a_{n,\nu}(k) i^n J_n(\kappa_{n,\nu} r) e^{in\varphi}. \quad (26)$$

Similarly, inserting Eq. (25) into Eq. (12) for  $i = 2$  gives

$$\Delta_{(r,\varphi)}\psi_2(r,\varphi) = \frac{1}{r^2} \left( r \frac{\partial}{\partial r} + i \frac{\partial}{\partial \varphi} \right) \left[ \frac{iz}{[w'(z)]^*} \frac{1}{k} \sum_{n,\nu} a_{n,\nu}(k) \kappa_{n,\nu}^2 i^n J_n(r\kappa_{n,\nu}) e^{i(n+1)\varphi} \right]$$

Assuming that the  $k$  value is chosen such that the condition Eq. (26) holds to replace the sum over  $n, \nu$  by the right-hand side of this equation, yields

$$\sum_{n,\nu} b_{n,\nu}(k) \kappa_{n,\nu}^2 i^{n+1} J_{n+1}(\kappa_{n,\nu} r) e^{i(n+1)\varphi} = \quad (28)$$

$$k^2 |w'(z)|^2 \sum_{n,\nu} b_{n,\nu}(k) i^{n+1} J_{n+1}(\kappa_{n,\nu} r) e^{i(n+1)\varphi} + \delta,$$

with  $\delta = 0$ . Yet, when this equation and Eq. (26) do not have solutions at the same values of  $k$ , then an additional term

$$\delta = 2ikw'(z)[w''(z)]^* \psi_1(r, \varphi) \quad (29)$$

appears in Eq. (28). Note, that these equations are no identities, but conditional equations for the eigenstates of the associated NB.

Defining in analogy to the nonrelativistic case, Eq. (19), matrices  $\hat{\mathcal{K}}_1, \hat{\mathcal{K}}_2, \hat{\mathcal{J}}_1$  and  $\hat{\mathcal{J}}_2$ , [cf. Eq. (S11) in Sec. A], Eqs. (26) and (28) can be written as

$$\left[ \hat{\mathcal{K}}_1 - k^2 \hat{\mathcal{J}}_1 \right] \mathbf{a} = 0, \quad (30)$$

$$\left[ \hat{\mathcal{K}}_2 - k^2 \hat{\mathcal{J}}_2 \right] \mathbf{b} = 0. \quad (31)$$

They have solutions only for discrete values of  $k = \tilde{k}_j$ , because the matrices  $\hat{\mathcal{K}}_1, \hat{\mathcal{K}}_2, \hat{\mathcal{J}}_1, \hat{\mathcal{J}}_2$  do not depend on  $k$ .

In [28]  $\mathbf{b}$  in Eq. (25) is set equal to  $\mathbf{a}$  in Eq. (24), thereby disregarding that their ansatz does not solve the Dirac equation (8) and (9), even not that for the circular NB. Then the eigenstates  $[\mathbf{a}_j(\tilde{k}_j), \tilde{k}_j]$  of the sum of Eqs. (30) and (31),  $\left[ \left( \hat{\mathcal{K}}_1 + \hat{\mathcal{K}}_2 \right) - \tilde{k}_j^2 \left( \hat{\mathcal{J}}_1 + \hat{\mathcal{J}}_2 \right) \right] \mathbf{a}_j = 0$ , are determined using the orthogonality Eq. (23),

$$\hat{\mathcal{J}} - \frac{\hat{\kappa}^2}{k^2} = \hat{0}, \quad \hat{\mathcal{J}}_{jj'} = \left( \mathcal{A}^T \left[ \hat{\mathcal{J}}_1 + \hat{\mathcal{J}}_2 \right] \mathcal{A} \right)_{jj'}, \quad (32)$$

$$\hat{\kappa}_{jj'}^2 = \left( \mathcal{A}^T \left[ \hat{\mathcal{K}}_1 + \hat{\mathcal{K}}_2 \right] \mathcal{A} \right)_{jj'} = \kappa_j^2 \delta_{jj'},$$

where the column vectors of the matrix  $\mathcal{A}$  are the eigenvectors  $\mathbf{a}_j$  corresponding to the eigenvalues  $\tilde{k}_j, j = 1, \dots, N$  and the dimension  $N$  equals the number of eigenstates of the circular NB,  $\kappa_1 \leq \kappa_2 \leq \dots \leq \kappa_N$ , taken into account. Yet, because of the assumption  $\mathbf{b} = \mathbf{a}$  in Eq. (25) these are no solutions of the Dirac equation (8) and (9). Indeed, these solutions deviate from those of Eq. (24) and of Eq. (25), and even for the case  $\mathbf{a} \neq \mathbf{b}$  these differ from each other [cf. Endmatter]. Accordingly, Eqs. (30), (31) for the spinor components and (32) do not have common solutions, implying

that the additional term  $\delta$  in Eq. (27) is nonzero, except for constant  $w'(z)$ , that is, for circular shapes. As mentioned above, the reason for this deficiency is that Eqs. (26) and (28) are no identities, as in the case of the ansatz Eq. (13) with Eq. (14), but conditional equations. Thus the spinors are no solutions of the Dirac equation for the corresponding NB.

Furthermore, the solutions of Eq. (32) ( $\tilde{k}_j, \psi_j(r, \varphi)$ ) do not fulfill the BC Eq. (5), namely

$$\psi_{1j}(r_0, \varphi) = i^{-1} e^{-i\varphi} \sum_{n,\nu} a_{n,\nu}(\tilde{k}_j) i^{n+1} J_{n+1}(r_0 \kappa_{n,\nu}) e^{i(n+1)\varphi}, \quad (33)$$

$$\neq \frac{1}{|w'(\varphi)|} \sum_{n,\nu} b_{n,\nu}(\tilde{k}_j) i^{n+1} J_{n+1}(r_0 \kappa_{n,\nu}) e^{i(n+1)\varphi}, \quad (34)$$

also not, when replacing  $b_{n,\nu}(\tilde{k}_j)/|w'(\varphi)|$  by  $a_{n,\nu}(\tilde{k}_j)$ . Here, the first equality results from the eigenvalue equation for circular NBs, Eq. (20), and can be written in the form  $\psi_1(\varphi) = -ie^{-i\varphi}\psi_2(\varphi)$ , and the second one corresponds to the BC Eq. (5). It obviously only holds for  $w'(\varphi) = ie^{i\varphi}, \tilde{k}_j = \kappa_{n,\nu}$ , implying that the outgoing flux is nonzero along the billiard boundary, namely

$$\mathbf{n} \cdot [\psi^\dagger \hat{\boldsymbol{\sigma}} \psi] = \cos[\alpha(\varphi)] \text{Re}[\psi_1^* \psi_2] + \sin[\alpha(\varphi)] \text{Im}[\psi_1^* \psi_2] \equiv \sin[\alpha(\varphi) - \varphi] |\psi_1(\varphi)|^2, \quad (35)$$

which is nonvanishing for NBs with non-circular shapes. Note that the effect of the boundary wave functions  $\psi_1(\varphi)$  and  $\psi_2(\varphi)$  remains non-negligible in the semiclassical limit  $k \rightarrow \infty$  [18]. This can be deduced from the fact, that in the trace formula, i.e. the semiclassical approximation for the spectral density in terms of a sum over of periodic orbits of the classical billiard of corresponding shape [36], those with an odd number of reflections [14, 37, 38] cancel each other when the spinor components are solutions of the Dirac equation for NBs. Note, that this feature of the trace formula is also observed in non-relativistic systems subject to a vectorial wave equation [39, 40]. This means that the size of the boundary wave functions  $|\psi_i(\varphi)|$  is generally comparable to that of the wave functions in the bulk.

The correct strategy to solve the Dirac equation (8) and (9) using the ansatz Eq. (24), would be to solve the generalized eigenvalue problem Eq. (30) for the first component, because for  $\mathbf{a} \neq \mathbf{b}$  the orthogonality of the eigenstates of the circular NB cannot be employed. Then the second component would be obtained from Eq. (25). Again, Eq. (30) has solutions only for discrete values of  $k$ , since the matrices  $\hat{\mathcal{J}}_i, \hat{\mathcal{K}}_i, i = 1, 2$  are assumed to be independent of  $k$ . However, as proven above, the solutions of Eqs. (28) and (26) differ for shapes with non-constant curvature and also the BC Eq. (5) is not fulfilled for non-circular shapes (cf. Endmatter). This discrepancy originates from the fact, that the BC for circular NBs is not the same as for NBs with a non-circular

shape, even though we restrict to shapes generated by applying a conformal map to a circle with radius  $r = r_0$ . Thus, the assumption, that the matrices entering the generalized eigenvalue problem Eq. (30) are independent of  $k$ , is not applicable. This is different from the case of non-relativistic billiards with the Dirichlet BC, which is independent of  $\varphi$  and fulfilled for each term in the associated expansion of the eigenstates in terms of those of the nonrelativistic circular QB [cf. Eq. (17)].

We conclude that the method proposed in [28, 29] for the determination of the eigenstates of NBs is only applicable to the circular NB, that is for the trivial case. Otherwise, it does not provide reliable solutions, because these do not comply with the Dirac equation and BCs for neutrino billiards. In these works the authors state that the solutions of the CMM fulfill the BC Eq. (5). Yet, for this the second spinor component  $\psi_{2j}(r, \varphi)$ , Eq. (25) needs to be multiplied with a  $\varphi$ -dependent factor, which can be read off Eqs. (33) and (34). However, even when the unmodified spinor components solve the Dirac equation, the modified ones do not fulfill it since application of the operator Eq. (7) to this factor is nonvanishing. This reflects the fact, that it is not sufficient to solve the Schrödinger equation for the spinor components, as demonstrated, e.g., for the ellipse NB in [41]. Due to the fact, that Eqs. (30) and (31) are not fulfilled simultaneously, in the semiclassical limit contributions of periodic orbits with an odd number of reflections – a feature attributed to the chirality of the solutions for NBs – won't cancel each other completely if the differences of their eigenvalues are large (see Ref. [18]).

In Ref. [30] the authors apply the same method to massive NBs with mass  $m_0 \neq 0$ . We demonstrate in Ref. [18], that the corresponding Dirac equation can be brought to the same form as in (8) and (9) with modified BCs that are shown to comply with the ultrarelativistic limit  $m_0 \rightarrow 0$  for massless NBs and the nonrelativistic limit,  $\frac{m_0 c}{\hbar k} \rightarrow \infty$ . Starting from this Dirac equation with modified BCs and proceeding as above, it can be shown, that the method of [30] does not provide the eigenstates of NBs with non-circular shapes.

In the Sec. IV we provide one example, which shows that the eigenvalues obtained from Eq. (32) can be close to those of the corresponding NB, for shapes with nearly constant curvature except in small parts of the boundary, however not the eigenfunctions, and another one, where this method fails. So as long as one is not interested in the eigenfunctions and their phases, and the shape is close to that of a circle, it can serve as an approximate method to determine a few 1000th of eigenvalues. On the other hand, the BIM introduced in Ref. [14] for the ultrarelativistic case and its extension to massive NBs [18, 42] yields at least that many eigenvalues with low numerical effort – especially for the NBs under consideration – and also the associated eigenfunctions with high precision. Thus, there is no reason to use a method, which has been proven to be erroneous and thus provides unreliable eigenstates. The flaws of the CMM unveiled in

this work, in fact explain the discrepancies between the solutions of the CMM and expected results observed, e.g. in Refs. [30, 31].

## IV. NUMERICAL STUDIES

### A. Numerical analysis of the CMM and BIM for billiards from a family whose shapes vary from circular to Africa

We compare results obtained with the CMM and the BIM, respectively, for a family of QBs and NBs [14, 35], whose shapes are given as

$$w^{AF}(z; \alpha) = \frac{z + \alpha z^2 + \alpha e^{i\pi/3} z^3}{\sqrt{1 + 5\alpha^2}}. \quad (36)$$

For  $\alpha = 0$  the shape is circular, whereas with increasing  $\alpha$  the classical dynamics undergoes a transition from regular via mixed regular-chaotic to chaotic. We computed eigenstates for several values of  $\alpha \leq 0.2$ . In Fig. 1 we show in the inset of the top part the shapes for  $\alpha = 0$  (black),  $\alpha = 0.1$  (blue),  $\alpha = 0.125$  (red) and  $\alpha = 0.2$ . For the latter one, known as 'Africa billiard', the dynamics is chaotic. Shown are the angle  $\alpha(s)$  of the normal vector with respect to the x-axis and the curvature  $\kappa(s)$  as function of the arclength parameter. The angle  $\alpha(s)$  varies nearly linearly with  $s$  and the curvature is close to unity, i.e. to that of a circle of radius unity, except in the regions around the two bulges.

To verify correctness of the codes used to solve Eqs. (30), (31) and (32), we first applied it to the corresponding QB, as the associated eigenvalue equations are similar to these equations. For the BIM the eigenvalues  $k_n$  and eigenfunctions are determined by solving a quantization condition of the form  $\det \hat{A}(k_n) = 0$ , where the matrix  $\hat{A}$  is obtained from a boundary-integral equation deduced from the Green theorem [14, 17, 18]. In the examples presented in the following we chose for the QB and NB the same dimension  $500 \times 500$  for  $\hat{A}$ , which corresponds to the discretization of the boundary into 500 pieces, and computed it for 600000 values of  $k$  in the range of  $k \in [0, 100]$  to obtain complete sequences of  $\approx 3000$  eigenvalues. For the CMM we considered in Eq. (17) 5000 eigenstates of the circular QB, yielding  $\simeq 2500$  reliable eigenvalues, as demonstrated in Fig. 1. There we compare the eigenvalues resulting from the BIM and CMM. For the NB we used the first 10000 eigenstates of the circular NB to compute the solutions of Eq. (30), Eq. (31) and Eq. (32). The number of eigenstates obtained from the CMM is of the same order as for the QB, even though we considered there only half the number of eigenstates of the circular QB. Beyond that value, the Weyl formula for NBs [14], which gives the average of the number of eigenvalues  $N(k_n)$  below  $k = k_n$ ,  $N^{Weyl}(k_n) = \frac{\mathcal{A}}{4\pi} k_n^2 + C$  with  $\mathcal{A}$  and  $C$  denoting the area of the corresponding NB and a positive constant  $C \lesssim 0.5$ ,

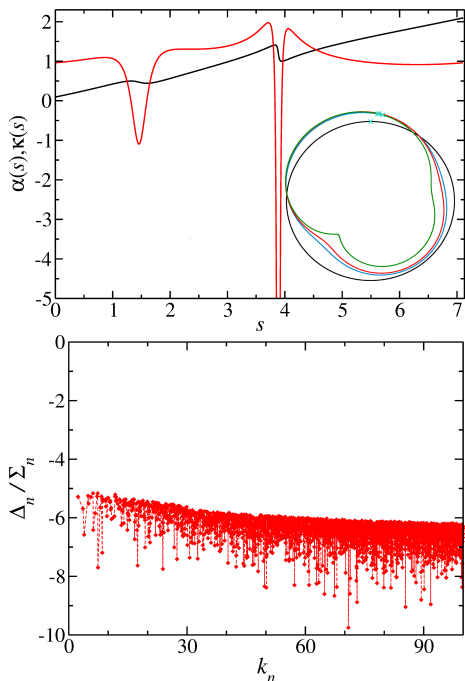


FIG. 1. Top: The angle  $\alpha(s)$  of the normal vector with respect to the  $x$  axis and boundary curvature for the shape of Africa billiard defined in Eq. (36) with  $\alpha = 0.2$ , with  $s$  denoting the arclength parameter. The shapes considered in this work are shown in the inset for  $\alpha = 0$  (black),  $\alpha = 0.1$  (blue),  $\alpha = 0.125$  (red) and  $\alpha = 0.2$  (green). The crosses mark the zero point of the arclength parameter  $s$ , which increases along the boundary in clockwise direction. Bottom: Relative differences  $\Delta_n / \Sigma_n = 2 \frac{|k_n^{BIM} - k_n^{CMM}|}{k_n^{BIM} + k_n^{CMM}}$  for the Africa QB with  $\alpha = 0.2$ . Here,  $k_n$ ,  $k_n^{BIM}$  and  $k_n^{CMM}$  denote the eigenvalues obtained with the BIM and CMM, respectively.

is no longer applicable [cf. the top part of Fig. 2] and the wave functions do not coincide with those expected for a NB. In fact, to compute the smooth part of  $N(k_n)$  we fit a polynomial of the form  $N^{smooth}(k_n) = \frac{\tilde{\mathcal{A}}}{4\pi} k_n^2 + \frac{\tilde{\mathcal{L}}}{4\pi} k_n + C$  to  $N(k_n)$ , which actually is the Weyl formula for non-relativistic QBs with area  $\tilde{\mathcal{A}}$  and perimeter  $\tilde{\mathcal{L}}$ . For the BIM the boundary term  $\frac{\tilde{\mathcal{L}}}{4\pi}$  is by a factor of  $10^{-5} - 10^{-4}$  smaller than the area term, whereas for the solutions of Eqs. (31) and (32) the factor increases from  $\approx 10^{-3}$  to  $\approx 10^{-2}$  with increasing deformation of the shape from that of a circle, and for the solutions of Eq. (30) this factor is about 10 times smaller than these values. Accordingly, for the CMM the parameter  $\tilde{\mathcal{A}}$  deviates by from the expected value,  $\mathcal{A}$ . In the bottom part of Fig. 2 we show the deviations of the eigenvalues obtained with the BIM from those computed from Eq. (32) (lower panels) and the arithmetic average of the solutions of Eqs. (30) and (31) (upper panels, black), respectively. The red dots in the upper panels show the spacings between the eigenvalues obtained from Eqs. (30) and (31). The distances are of similar size for all cases and by at least two decades larger than for the nonrelativistic case, thus confirming

that the CMM does not yield solutions of the Dirac equation for NBs. Still, the agreement with the eigenvalues obtained from the exact quantization procedure, i.e., the BIM is good, especially for the solutions of Eq. (30), even for the case with  $\alpha = 0.2$  as maybe explained by the fact that the boundary curvature is close to that of the circle except in the region around the bulges. However, generally, as demonstrated in Fig. 2, the deviations between the eigenvalues obtained with the BIM and CMM increase with the deformation of the circular NB, thus corroborating the proof.

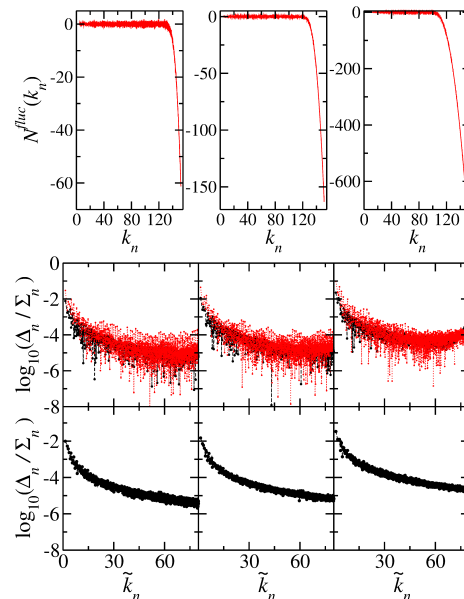


FIG. 2. Top: Difference  $N^{fluc}(k_n) = N(k_n) - N^{Weyl}(k_n)$  between the number of eigenvalues  $N(k_n)$  below  $k = k_n$  and the Weyl formula  $N^{Weyl}(k_n) = \frac{\mathcal{A}}{4\pi} k_n^2 + C$  for the NB with  $\alpha = 0.1$  (left),  $\alpha = 0.125$  (middle) and  $\alpha = 0.2$  (right). Bottom: Relative differences  $\Delta_n / \Sigma_n = 2 \frac{|k_n^a - k_n^b|}{k_n^a + k_n^b}$  for the Africa NB with  $\alpha = 0.1$  (left),  $\alpha = 0.125$  (middle) and  $\alpha = 0.2$  (right). In the upper panels are shown the distances between the eigenvalues obtained from the BIM and the arithmetic mean of those obtained from Eqs. (30) and (31) (black) and the distances between the latter two (red). In the lower panels are shown the distances between the eigenvalues resulting from the BIM and those obtained with Eq. (32).

Furthermore, the boundary wave functions, shown in Fig. S1 of Sec. A for the BIM and CMM cases, show clear differences. Note, that the period of the observed oscillations is determined by the perimeter of the billiard and by the wave length, which is similar for both cases. The outgoing flux is of the order of  $10^{-16}$  for the BIM results and agrees well with the analytical result Eq. (35) for the CMM ones. A clear discrepancy is visible for all cases also in the wave functions shown in Fig. S2 of Sec. A, one reason being that their phases differ due to the differing boundary conditions. The wave functions for state 2508 are scarred along a straight line corresponding to a remnant of the diameter orbit in the original circular

NB. It bounces back and forth between two nearly circular focussing boundary segments, and thus is expected to occur in both cases, with dominant support in the region where the boundary curvature is close to unity. Indeed, such scarred wave functions are also observed in the Africa QB. Nevertheless, to get for the CMM case the correct phase along that orbit, the wave function has to be multiplied with a factor in order to fulfill the BC for the NB [cf. Eq. (34)].

### B. Example of a billiard for which the shape deviates from that of the circular NB

We also considered two billiards with shapes given by Eq. (6) with  $c_1 = 1$ ,  $c_2 = c_4 = c_5 = 0.1$ , and  $c_3 = 0.1 - i$  – exhibiting a mirror symmetry –, respectively,  $c_3 = 0.1e^{i\pi/3}$  – deviating along most parts of the boundary from that of a circle. The shapes are shown in the insets of the top and bottom part of Fig. 3, respectively. To obtain the solutions of Eqs. (30), (31) and (32) we used the same number of eigenvalues of the corresponding circular QB and NB as in the previous examples. However, in that case only about 1000 eigenvalues could be obtained that comply with the Weyl formula in the sense that the smooth part of the integrated spectral density is well described by the second-order polynomial given above [cf. top part of Fig. 4]. Namely  $\tilde{\mathcal{L}}$  is by a factor  $10^{-5}$  smaller than the area term for the BIM, whereas for the solutions of Eqs. (31) and (32) this factor is  $\approx 10^{-2}$  and  $\approx 10^{-1}$  for complex and real  $c_3$ , respectively, and for the solutions of Eq. (30) about 10 times smaller than these values. It can be seen in Fig. 3 that the solutions of Eqs. (30), (31) and (32) clearly deviate from each other, also the arithmetic averages of the eigenvalues obtained from Eqs. (30) and (31) differ from those computed with Eq. (32), thus demonstrating that the assumption that the eigenvalues of the NB can be obtained from the sum of Eqs. (30) and (31) with  $\mathbf{a} = \mathbf{b}$  is wrong. They also deviate from those obtained with the BIM for the corresponding NB, as exhibited in the bottom part of Fig. 4. The high accuracy of the eigenvalues computed with the BIM can be deduced from the fact, that  $\tilde{\mathcal{A}} = \mathcal{A} + o(10^{-6})$  and  $\tilde{\mathcal{L}} \sim 10^{-6}$ . Furthermore, to get an estimate for the size of deviations we also show the differences between the eigenvalues  $k_n^a = \tilde{k}_n$  of the corresponding QB, computed with the BIM and the CMM Eq. (18). These are a factor  $10^{-3}$  smaller than for the NB. The spectral properties are close to GUE for the eigenvalues of the billiard with complex  $c_3$ , whereas they are close to the GOE for the shape with real  $c_3$ . This is expected, because for that case the shape has a mirror symmetry. However, in contrast to the non-relativistic QB, the associated eigenstates cannot be separated according to their mirror symmetry, so the BIM and also the CMM should be applied to the whole billiard system. Yet, the spectral properties of the eigenvalues obtained from Eqs. (32), (30) and (31) clearly deviate from each other, thus corroborating the analyti-

cal proofs of non-applicability of the CMM for relativistic quantum billiards, provided in the main text.

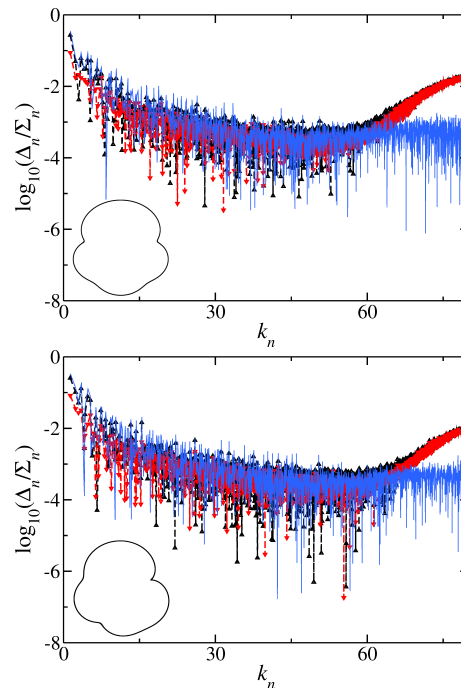


FIG. 3. Top: Relative differences  $\Delta_n/\Sigma_n = 2 \frac{|k_n^a - k_n^b|}{k_n^a + k_n^b}$  between the eigenvalues  $k_n^a$  obtained from Eq. (31) and  $k_n^b$  from Eq. (32) (black), between the arithmetic average of the eigenvalues obtained from Eqs. (30) and (31)  $k_n^a$ , and  $k_n^b$  from Eq. (32) (red), and between the eigenvalues  $k_n^a$  obtained from Eq. (30) and  $k_n^b$  from Eq. (31) (blue) for the billiard with  $c_3$  real, shown in the inset. Bottom: same as top for the shape shown in the inset.

## V. CONCLUSIONS

In [28] and subsequent works of these authors, the CMM is applied to NBs, namely the Schrödinger equation Eq. (12) is solved for the sum of the spinor components, using for them expansions in terms of the corresponding component of the eigenstates of a circular NB with same expansion coefficient. By doing so the authors assume that the corresponding Schrödinger equations for the two spinor components have the same solutions, and above all ignore their relation through the associated Dirac equation. The solutions fulfill by construction the BC of that circular NB, namely, the outgoing flow vanishes along the boundary of the circle. We demonstrate in the Endmatter also numerically that the solutions of the equations (26) and (28) are not the same and they also do not coincide with those for their sum. Thus it is questionable to what extent these solutions of the Schrödinger equation for nonrelativistic QBs, are connected to those of relativistic quantum billiards. Note, that the resulting wave functions are complex, since the ansatz spinors are,

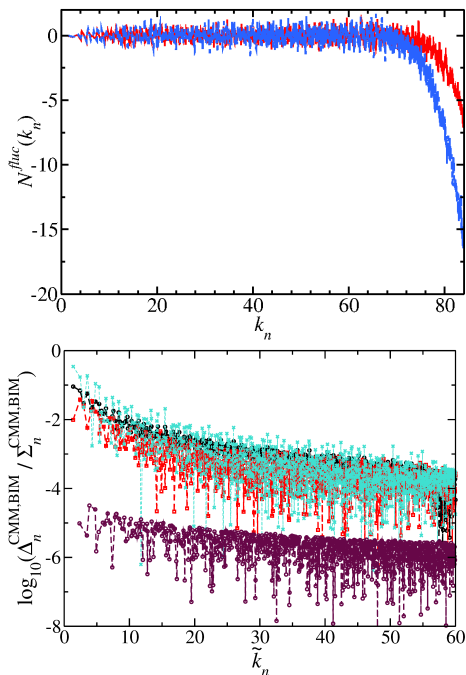


FIG. 4. Top: Difference  $N^{fluc}(k_n) = N(k_n) - N^{smooth}(k_n)$  between the number of eigenvalues  $N(k_n)$  below  $k = k_n$  and the the best fitting Weyl formula  $N^{smooth}(k_n) = \frac{\tilde{A}}{4\pi} k_n^2 + \frac{\tilde{C}}{4\pi} k_n + C$  for QBs for the billiard with real (blue) and complex (red)  $c_{3i}$  [cf. insets of top and bottom part of Fig. 3]. Bottom: Relative differences  $\Delta_n/\Sigma_n = 2 \frac{|k_n^a - k_n^b|}{k_n^a + k_n^b}$  between the eigenvalues  $k_n^a = \tilde{k}_n$  obtained for the NB with shape shown in the bottom part of Fig. 3 using the BIM and  $k_n^b$  obtained from Eqs. (32) (black), from (30) (red) and from Eq. (31) (turquoise) and for the corresponding QB with eigenvalues  $k_n^a = \tilde{k}_n$  computed with the BIM and those obtained from Eq. (18) (maroon).

that is they are not invariant under time-reversal. Furthermore, like in the nonrelativistic CMM, the potential  $|w'(z)|^2$  induces a chaotic dynamics if the shape of the NB is chosen accordingly, so the spectral properties are expected to coincide with those of the NB, even though the eigenstates differ.

## VI. ACKNOWLEDGEMENT

The author acknowledges financial support from the Institute for Basic Science in Korea through the project IBS-R024-D1.

### Appendix A: Appendix

In the appendix some technical details, employed in the main text, are provided, and examples of wave functions are shown.

#### 1. Some technical details

The plane-wave expansion for the second component Eq. (14) in the main text is obtained by inserting the ansatz for the first component, Eq. (13) into Eq. (9) and employing the equalities

$$\frac{1}{z^*[w'(z)]^*} \left( r \frac{\partial}{\partial r} + i \frac{\partial}{\partial \varphi} \right) |w(z)| = e^{i\theta(z)}, \quad (\text{A1})$$

$$\begin{aligned} \frac{1}{z^*[w'(z)]^*} \left( r \frac{\partial}{\partial r} + i \frac{\partial}{\partial \varphi} \right) e^{il\theta(z)} &= -\frac{l}{|w(z)|} e^{i(l+1)\theta(z)}, \\ \frac{1}{zw'(z)} \left( r \frac{\partial}{\partial r} - i \frac{\partial}{\partial \varphi} \right) e^{il\theta(z)} &= \frac{l}{|w(z)|} e^{i(l-1)\theta(z)}, \end{aligned} \quad (\text{A2})$$

and

$$J_{l-1}(x) = \frac{l}{x} J_l(x) + \frac{dJ_l(x)}{dx}, \quad J_{l+1}(x) = \frac{l}{x} J_l(x) - \frac{dJ_l(x)}{dx}. \quad (\text{A3})$$

The spinor eigenfunction,

$$\Phi_{n,\nu}(r, \varphi) = \begin{pmatrix} \Phi_{1n,\nu}(r, \varphi) \\ \Phi_{2n,\nu}(r, \varphi) \end{pmatrix}, \quad (\text{A4})$$

are orthogonal to each other,

$$\int_0^{r_0} r dr \int_0^{2\pi} d\varphi \Phi_{m,\mu}(r, \varphi) \cdot \Phi_{n,\nu}(r, \varphi) \quad (\text{A5})$$

$$= \delta_{n,m} 2\pi \int_0^{r_0} r dr [J_{m,\mu}(\kappa_{m,\mu} r) J_{m,\nu}(\kappa_{m,\nu} r) + J_{m+1,\mu}(\kappa_{m,\mu} r) J_{m+1,\nu}(\kappa_{m,\nu} r)] \mathcal{N}_{m,\mu} \mathcal{N}_{m,\nu} \quad (\text{A6})$$

$$\propto \delta_{n,m} \delta_{\nu,\mu}. \quad (\text{A7})$$

Namely, for  $\Phi_{1n,\nu}(r, \varphi)$  we have

$$\begin{aligned} & \int_0^{r_0} r dr \int_0^{2\pi} d\varphi J_n(\kappa_{n,\nu} r) J_m(\kappa_{m,\mu} r) e^{i(n-m)\varphi}, \quad (\text{A8}) \\ &= 2\pi \delta_{n,m} \frac{\kappa_{m,\nu} r_0 J_{m+1}(\kappa_{m,\nu} r_0) J_m(\kappa_{m,\mu} r_0) - \kappa_{m,\mu} r_0 J_{m+1}(\kappa_{m,\mu} r_0) J_m(\kappa_{m,\nu} r_0)}{\kappa_{m,\nu}^2 - \kappa_{m,\mu}^2}, \\ &= 2\pi \delta_{n,m} \begin{cases} \frac{J_m(\kappa_{m,\nu} r_0) J_m(\kappa_{m,\mu} r_0)}{\kappa_{m,\nu} + \kappa_{m,\mu}} & , \nu \neq \mu \\ -r_0^2 J_m(\kappa_{m,\mu} r_0) J'_{m,\mu}(\kappa_{m,\mu} r_0) & , \nu = \mu \end{cases} \end{aligned}$$

and similarly for  $\Phi_2(r, \varphi)$

$$\begin{aligned} & \int_0^{r_0} r dr \int_0^{2\pi} d\varphi J_{n+1}(\kappa_{n,\nu} r) J_{m+1}(\kappa_{m,\mu} r) e^{i(n-m)\varphi}, \quad (\text{A9}) \\ &= 2\pi \delta_{n,m} \frac{\kappa_{m,\mu} r_0 J_m(\kappa_{m,\mu} r_0) J_{m+1}(\kappa_{m,\nu} r_0) - \kappa_{m,\nu} r_0 J_m(\kappa_{m,\nu} r_0) J_{m+1}(\kappa_{m,\mu} r_0)}{\kappa_{m,\nu}^2 - \kappa_{m,\mu}^2}, \\ &= 2\pi \delta_{n,m} \begin{cases} \frac{-J_m(\kappa_{m,\nu} r_0) J_m(\kappa_{m,\mu} r_0)}{\kappa_{m,\nu} + \kappa_{m,\mu}} & , \nu \neq \mu \\ r_0^2 J_m(\kappa_{m,\mu} r_0) J'_{(m+1),\mu}(\kappa_{m,\mu} r_0) & , \nu = \mu \end{cases} \end{aligned}$$

where we employed the BC Eq. (20) in the main text, implying that for  $\nu \neq \mu$  the sum of the contributions from the two spinor components cancel each other and

$$\frac{1}{\mathcal{N}_{m,\mu} \mathcal{N}_{n,\nu}} \int_0^{r_0} r dr \int_0^{2\pi} d\varphi \Phi_{m,\mu}(r, \varphi) \cdot \Phi_{n,\nu}(r, \varphi) = \delta_{n,m} \delta_{\nu,\mu} \pi r_0^2 \left[ \frac{dJ_{(m+1),\mu}^2(x)}{dx} - \frac{dJ_{m,\mu}^2(x)}{dx} \right] \Big|_{(x=\kappa_{m,\mu})} = \frac{1}{\mathcal{N}_{n,\nu}^2}. \quad (\text{A10})$$

In analogy to the nonrelativistic case, Eq. (19) in the main text, the matrices  $\hat{\mathcal{K}}_1$ ,  $\hat{\mathcal{K}}_2$ ,  $\hat{\mathcal{J}}_1$  and  $\hat{\mathcal{J}}_2$ , are defined as

$$\begin{aligned} \hat{\mathcal{K}}_{1;jj'} &= 2\pi \delta_{nm} \mathcal{N}_{n,\nu} \mathcal{N}_{m,\mu} \int_0^{r_0} r dr J_m(\kappa_{m,\mu} r) J_m(\kappa_{m,\nu} r) \kappa_{m,\nu}^2, \quad (\text{A11}) \\ \hat{\mathcal{K}}_{2;jj'} &= 2\pi \delta_{nm} \mathcal{N}_{n,\nu} \mathcal{N}_{m,\mu} \int_0^{r_0} r dr J_{m+1}(\kappa_{m,\mu} r) J_{m+1}(\kappa_{m,\nu} r) \kappa_{m,\nu}^2, \\ \hat{\mathcal{J}}_{1;jj'} &= \mathcal{N}_{n,\nu} \mathcal{N}_{m,\mu} \int_0^{r_0} r dr \int_0^{2\pi} d\varphi |w'(z)|^2 J_m(\kappa_{m,\mu} r) J_n(\kappa_{n,\nu} r) i^{(n-m)} e^{i(n-m)\varphi}, \\ \hat{\mathcal{J}}_{2;jj'} &= \mathcal{N}_{n,\nu} \mathcal{N}_{m,\mu} \int_0^{r_0} r dr \int_0^{2\pi} d\varphi |w'(z)|^2 J_{m+1}(\kappa_{m,\mu} r) J_{n+1}(\kappa_{n,\nu} r) i^{(n-m)} e^{i(n-m)\varphi}, \end{aligned}$$

with  $[m, \mu] = [l(j), \lambda(j)]$ ,  $[n, \nu] = [l(j'), \lambda(j')]$ .

## 2. Comparison of wave functions obtained from CMM and BIM

In Figs. A1 and A2 are shown examples of boundary wave functions and wave functions obtained with the BIM and CMM, respectively.

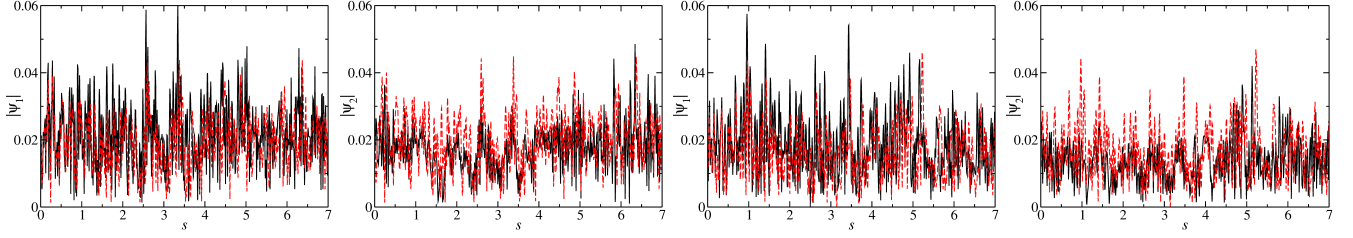


FIG. A1. Modulus of the boundary functions from left to right for first and second component of eigenstate 2507 and for first and second component of eigenstate 2508 for the solutions of the BIM (black) and the CMM (red dashed).

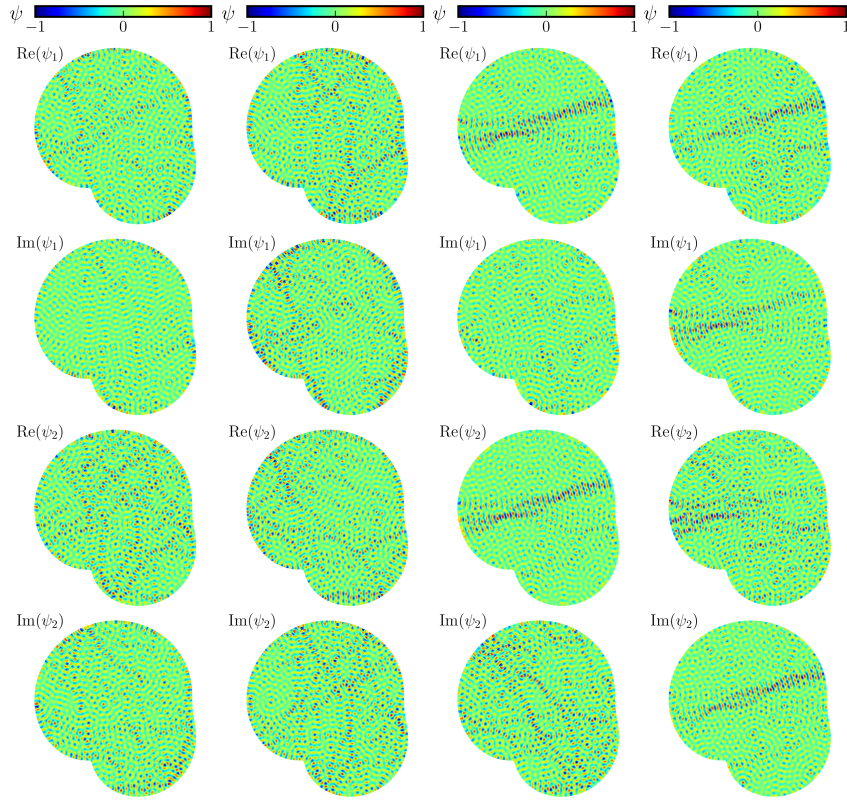


FIG. A2. Real and Imaginary parts of the spinor wave functions obtained from the BIM (1st and 3rd column) and CMM (2nd and 4th column) for the eigenstate 2507 (left pair of columns) and 2508 (right pair of column).

- 
- [1] Y. G. Sinai, Dynamical systems with elastic reflections, *Russ. Math. Surv.* **25**, 137 (1970).  
 [2] L. A. Bunimovich, On the ergodic properties of nowhere dispersing billiards, *Commun. Math. Phys.* **65**, 295 (1979).

- [3] M. V. Berry, Regularity and chaos in classical mechanics, illustrated by three deformations of a circular 'billiard', *Eur. J. Phys.* **2**, 91 (1981).  
 [4] M. Giannoni, A. Voros, and J. Zinn-Justin, eds., *Chaos and Quantum Physics* (Elsevier, Amsterdam, 1989).

- [5] H.-J. Stöckmann and J. Stein, "quantum" chaos in billiards studied by microwave absorption, *Phys. Rev. Lett.* **64**, 2215 (1990).
- [6] A. Richter, Playing billiards with microwaves - quantum manifestations of classical chaos, in *Emerging Applications of Number Theory*, The IMA Volumes in Mathematics and its Applications, Vol. 109, edited by D. A. Hejhal, J. Friedman, M. C. Gutzwiller, and A. M. Odlyzko (Springer, New York, 1999) p. 479.
- [7] F. H. and, *Quantum Signatures of Chaos* (Springer-Verlag, Heidelberg, 2001).
- [8] S. Sridhar, Experimental observation of scarred eigenfunctions of chaotic microwave cavities, *Phys. Rev. Lett.* **67**, 785 (1991).
- [9] H.-D. Gräf, H. L. Harney, H. Lengers, C. H. Lewenkopf, C. Rangacharyulu, A. Richter, P. Schardt, and H. A. Weidenmüller, Distribution of eigenmodes in a superconducting stadium billiard with chaotic dynamics, *Phys. Rev. Lett.* **69**, 1296 (1992).
- [10] J. Stein and H.-J. Stöckmann, Experimental determination of billiard wave functions, *Phys. Rev. Lett.* **68**, 2867 (1992).
- [11] P. So, S. M. Anlage, E. Ott, and R. Oerter, Wave chaos experiments with and without time reversal symmetry: GUE and GOE statistics, *Phys. Rev. Lett.* **74**, 2662 (1995).
- [12] S. Deus, P. M. Koch, and L. Sirko, Statistical properties of the eigenfrequency distribution of three-dimensional microwave cavities, *Phys. Rev. E* **52**, 1146 (1995).
- [13] B. Dietz and A. Richter, Quantum and wave dynamical chaos in superconducting microwave billiards, *Chaos* **25**, 097601 (2015).
- [14] M. V. Berry and R. J. Mondragon, Neutrino billiards: Time-reversal symmetry-breaking without magnetic fields, *Proc. R. Soc. London A* **412**, 53 (1987).
- [15] V. Heuveline, On the computation of a very large number of eigenvalues for selfadjoint elliptic operators by means of multigrid methods, *J. Comput. Phys.* **184**, 321 (2003).
- [16] E. Vergini and M. Saraceno, Calculation by scaling of highly excited states of billiards, *Phys. Rev. E* **52**, 2204 (1995).
- [17] A. Bäcker, Numerical Aspects of Eigenvalue and Eigenfunction Computations for Chaotic Quantum Systems, in *The Mathematical Aspects of Quantum Maps*, edited by M. D. Esposti and S. Graffi (Springer Berlin Heidelberg, Berlin, Heidelberg, 2003) pp. 91–144.
- [18] B. Dietz and Z.-Y. Li, Semiclassical quantization of neutrino billiards, *Phys. Rev. E* **102**, 042214 (2020).
- [19] B. Dietz and A. Richter, Intermediate statistics in singular quarter-ellipse shaped microwave billiards\*, *J. Phys. A: Math. Theor.* **55**, 314001 (2022).
- [20] J. Wiersig, Boundary element method for resonances in dielectric microcavities, *J. Opt. A: Pure Appl. Opt.* **5**, 53 (2002).
- [21] R. Ketzmerick, F. Lorenz, and J. R. Schmidt, Semiclassical limit of resonance states in chaotic scattering, *Phys. Rev. Lett.* **134**, 020404 (2025).
- [22] C.-H. Yi, B. Dietz, J.-H. Han, and J.-W. Ryu, Decay rates of optical modes unveil the island structures in mixed phase space (2025), arXiv:2502.07407 [physics.optics].
- [23] Y. Okada, A. Shudo, S. Tasaki, and T. Harayama, On the boundary element method for billiards with corners, *J. Phys. A: Math. Gen.* **38**, 6675 (2005).
- [24] G. Veble, T. Prosen, and M. Robnik, Expanded boundary integral method and chaotic time-reversal doublets in quantum billiards, *New J. Phys.* **9**, 15 (2007).
- [25] P. Yu, B. Dietz, and L. Huang, Quantizing neutrino billiards: an expanded boundary integral method, *New J. Phys.* **21**, 073039 (2019).
- [26] B. Dietz, Semi-Poisson statistics in relativistic quantum billiards with shapes of rectangles, *Entropy* **25**, 10.3390/e25050762 (2023).
- [27] M. Robnik, Quantising a generic family of billiards with analytic boundaries, *J. Phys. A: Math. Gen.* **17**, 1049 (1984).
- [28] H. Xu, L. Huang, Y.-C. Lai, and C. Grebogi, Chiral scars in chaotic dirac fermion systems, *Phys. Rev. Lett.* **110**, 064102 (2013).
- [29] L. Huang, H.-Y. Xu, C. Grebogi, and Y.-C. Lai, Relativistic quantum chaos, *Phys. Rep.* **753**, 1 (2018).
- [30] M.-Y. Song, Z.-Y. Li, H.-Y. Xu, L. Huang, and Y.-C. Lai, Quantization of massive Dirac billiards and unification of nonrelativistic and relativistic chiral quantum scars, *Phys. Rev. Research* **1**, 033008 (2019).
- [31] Z.-Y. Li, L.-L. Ye, R.-H. Ni, C.-Z. Wang, L. Huang, Y.-C. Lai, and C. Grebogi, Relativistic quantum scarring, spin-induced phase, and quantization in a symmetric dirac billiard system, *J. Phys. A: Math. Theor.* **55**, 374003 (2022).
- [32] H. Weyl, *Elektron und Gravitation. I*, *Z. Physik* **56**, 330 (1929).
- [33] This choice of BCs is not the only one guaranteeing self-adjointness of the Dirac Hamiltonian and zero outgoing current [43, 44].
- [34] B. Dietz and U. Smilansky, A scattering approach to the quantization of billiards—the inside–outside duality, *Chaos* **3**, 581 (1993).
- [35] M. V. Berry and M. Robnik, Statistics of energy levels without time-reversal symmetry: Aharonov-Bohm chaotic billiards, *J. Phys. A* **19**, 649 (1986).
- [36] M. C. Gutzwiller, Periodic orbits and classical quantization conditions, *J. Math. Phys.* **12**, 343 (1971).
- [37] J. Bolte and S. Keppeler, A semiclassical approach to the Dirac equation, *Ann. Phys.* **274**, 125 (1999).
- [38] J. Wurm, A. Rycerz, Ī. Adagideli, M. Wimmer, K. Richter, and H. U. Baranger, Symmetry classes in graphene quantum dots: Universal spectral statistics, weak localization, and conductance fluctuations, *Phys. Rev. Lett.* **102**, 056806 (2009).
- [39] R. Balian and B. Duplantier, Electromagnetic waves near perfect conductors. I. Multiple scattering expansions. Distribution of modes, *Ann. Phys. (N.Y.)* **104**, 300 (1977).
- [40] C. Dembowski, B. Dietz, H.-D. Gräf, A. Heine, T. Papenbrock, A. Richter, and C. Richter, Experimental test of a trace formula for a chaotic three-dimensional microwave cavity, *Phys. Rev. Lett.* **89**, 064101 (2002).
- [41] B. Dietz, Circular and elliptical neutrino billiards: A semiclassical approach, *Act. Phys. Pol. A* **136**, 770 (2019).
- [42] B. Dietz, Unidirectionality and Husimi functions in constant-width neutrino billiards, *J. Phys. A: Math. Theor.* **55**, 474003 (2022).
- [43] W. A. Gaddah, Exact solutions to the Dirac equation for equilateral triangular billiard systems, *J. Phys. A: Math. Theor.* **51**, 385304 (2018).
- [44] W. Greiner and A. Schäfer, eds., *Quantum Chromody-*

*namics* (Springer, New York, 1994).